

Electron doping evolution of the anisotropic spin excitations in $\text{BaFe}_{2-x}\text{Ni}_x\text{As}_2$ Huiqian Luo,¹ Zahra Yamani,² Yanchao Chen,¹ Xingye Lu,^{1,3} Meng Wang,¹ Shiliang Li,¹ Thomas A. Maier,⁴ Sergey Danilkin,⁵ D. T. Adroja,⁶ and Pengcheng Dai^{3,1,*}¹*Beijing National Laboratory for Condensed Matter Physics, Institute of Physics, Chinese Academy of Sciences, Beijing 100190, China*²*Canadian Neutron Beam Centre, National Research Council, Chalk River Laboratories, Chalk River, Ontario K0J 1J0, Canada*³*Department of Physics and Astronomy, The University of Tennessee, Knoxville, Tennessee 37996-1200, USA*⁴*Computer Science and Mathematics Division and Center for Nanophase Materials Sciences, Oak Ridge National Laboratory, Oak Ridge, Tennessee 37831, USA*⁵*Bragg Institute, Australian Nuclear Science and Technology Organization, New Illawarra Road, Lucas Heights NSW-2234, Australia*⁶*ISIS Facility, Rutherford Appleton Laboratory, Chilton, Didcot, Oxfordshire OX11 0QX, United Kingdom*

(Received 24 May 2012; published 10 July 2012)

We use inelastic neutron scattering to systematically investigate the Ni-doping evolution of the low-energy spin excitations in $\text{BaFe}_{2-x}\text{Ni}_x\text{As}_2$ spanning from underdoped antiferromagnet to overdoped superconductor ($0.03 \leq x \leq 0.18$). In the undoped state, BaFe_2As_2 changes from paramagnetic tetragonal phase to orthorhombic antiferromagnetic (AF) phase below about 138 K, where the low-energy ($\leq \sim 80$ meV) spin waves form transversely elongated ellipses in the $[H, K]$ plane of the reciprocal space. Upon Ni doping to suppress the static AF order and induce superconductivity, the c -axis magnetic exchange coupling is rapidly suppressed and the momentum distribution of spin excitations in the $[H, K]$ plane is enlarged in both the transverse and longitudinal directions with respect to the in-plane AF ordering wave vector of the parent compound. As a function of increasing Ni-doping x , the spin excitation widths increase linearly but with a larger rate along the transverse direction. These results are in general agreement with calculations of dynamic susceptibility based on the random phase approximation (RPA) in an itinerant electron picture. For samples near optimal superconductivity at $x \approx 0.1$, a neutron spin resonance appears in the superconducting state. Upon further increasing the electron doping to decrease the superconducting transition temperature T_c , the intensity of the low-energy magnetic scattering decreases and vanishes concurrently with vanishing superconductivity in the overdoped side of the superconducting dome. Comparing with the low-energy spin excitations centered at commensurate AF positions for underdoped and optimally doped materials ($x \leq 0.1$), spin excitations in the overdoped side ($x = 0.15$) form transversely incommensurate spin excitations, consistent with the RPA calculation. Therefore, the itinerant electron approach provides a reasonable description to the low-energy AF spin excitations in $\text{BaFe}_{2-x}\text{Ni}_x\text{As}_2$.

DOI: [10.1103/PhysRevB.86.024508](https://doi.org/10.1103/PhysRevB.86.024508)

PACS number(s): 74.25.Ha, 74.70.-b, 78.70.Nx

I. INTRODUCTION

Spin excitations are thought to be a candidate for mediating the electron pairing for superconductivity in unconventional superconductors.^{1,2} For copper oxide high-transition temperature (high- T_c) superconductors, superconductivity arises from charge carrier doping of their antiferromagnetic (AF) Mott insulating parent compounds and forms a superconducting (SC) dome including underdoped, optimally doped, and overdoped materials.³ Although static AF order is suppressed in optimally doped superconductors, spin excitations persist throughout the SC dome and vanish when superconductivity ceases to exist in the overdoped materials.⁴ These results provided compelling evidence that SC electrons in copper oxides are intimately associated with spin excitations,⁵ and spin excitations may mediate electron pairing for superconductivity.⁶ For iron pnictides,⁷⁻¹⁰ superconductivity can also be induced from the electron or hole doping of their AF ordered metallic parent compounds.¹¹⁻¹³ Because the parent compounds of iron pnictide superconductors are metallic with hole and electron Fermi surfaces centered at Γ and M points of the reciprocal space, respectively, the AF order and superconductivity may arise from quasiparticle excitations between the hole and electron pockets,¹⁴⁻¹⁸ much different from the local moment Mott physics of copper oxides.³ In the electron itinerant picture, the AF order in the parent compounds arises from

Fermi surface nesting of the hole and electron pockets. Since the electron doping that induces superconductivity also increases the size of the electron pocket near M points and reduces the hole-pocket size near Γ points, the static AF order is gradually suppressed with increasing electron doping, and superconductivity emerges from the signed reversed quasiparticles excitations between the hole and electron pockets.¹⁴⁻¹⁸ As a consequence of opening up the electronic gaps at the hole (Δ_h) and electron (Δ_e) Fermi pockets in the SC state, a neutron spin resonance is expected to occur at the AF nesting wave vector with an energy $E \leq 2\Delta = (|\Delta_h| + |\Delta_e|)$.¹⁹⁻²¹ Indeed, inelastic neutron scattering experiments on single crystals of electron-doped $\text{BaFe}_{2-x}\text{T}_x\text{As}_2$ ($T = \text{Co}, \text{Ni}$, see inset in Fig. 1 for the crystal structure) confirm the presence of the resonance.²²⁻³³ In particular, recent time-of-flight inelastic neutron scattering measurements reveal that the high-energy ($E > 100$ meV) spin waves in the non-SC BaFe_2As_2 persist into the SC $\text{BaFe}_{1.9}\text{Ni}_{0.1}\text{As}_2$, and the effect of electron doping is to form the resonance and modify the low-energy spin excitations.³⁴

If we assume that the high-energy spin excitations are due to localized moments and electron doping only affects the Fermi surface nesting and low-energy spin excitations,³⁴ one can make a direct comparison between the measured neutron scattering wave vector profiles and results from

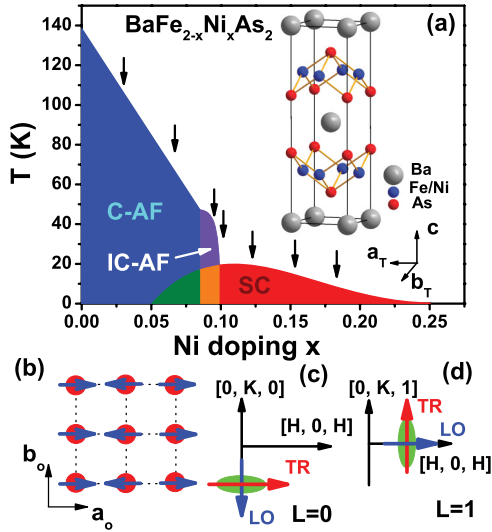


FIG. 1. (Color online) (a) The electronic phase diagram and crystal structure of $\text{BaFe}_{2-x}\text{Ni}_x\text{As}_2$. The arrows indicate seven doping levels studied in this experiment. (b) the colinear AF structure in the FeAs-plane of $\text{BaFe}_{2-x}\text{Ni}_x\text{As}_2$. (c) and (d) Schematic pictures of constant-energy scans along transverse (TR) and longitudinal (LO) directions both at $L = 0$ and $L = 1$.

the random phase approximation (RPA) calculations of the three-dimensional tight-binding model in the local density approximation (LDA).³⁵ For example, the transversely elongated ellipses of the resonance in the electron-doped $\text{BaFe}_{2-x}\text{As}_2$ ^{29–31,34} from the spin waves in BaFe_2As_2 ³⁶ due to the enhancement of the intraorbital, but interband, pair scattering process between the d_{xy} orbitals have been interpreted as being more effective in giving rise to the fully gapped S^\pm -symmetry superconductivity.³⁷ The density-functional-theory (DFT) calculations³⁰ had also predicted correctly that the momentum anisotropy of the neutron spin resonance in the optimally hole-doped materials is rotated by 90° from that of the electron-doped case and becomes the longitudinally elongated ellipse.³⁸ Moreover, the effect of Fermi surface nesting appears to account for the hole-doping evolution of the spin excitations in $\text{Ba}_{1-x}\text{K}_x\text{Fe}_2\text{As}_2$.³⁹ Finally, recent neutron diffraction work has established, within a narrow region of x in $\text{BaFe}_{2-x}\text{As}_2$ [Fig. 1(a)], elastic transversely incommensurate short-range magnetic peaks that have been hailed as direct evidence for the spin-density-wave order due to mismatch of the hole-electron pocket Fermi surface nesting.^{40–42}

Given that the RPA/DFT calculations have so much success in describing the elastic magnetic scattering and low-energy spin excitations in $\text{BaFe}_{2-x}\text{As}_2$, it is surprising that there are still no quantitative comparison of the doping dependence of the spin excitation profiles with systematic RPA/DFT calculations. In particular, while DFT calculations predicted that spin excitations in 7.5% electron-doped $\text{BaFe}_{2-x}\text{As}_2$ should be incommensurate along the transverse direction, low-energy spin excitations seen by neutron scattering show only commensurate scattering with transversely elongated ellipses.^{29–31,34} Since one can systematically carry out RPA/DFT calculations to obtain the imaginary part of the dynamic susceptibility, $\chi''(\mathbf{Q}, \omega)$, as a function of electron-

doping x in $\text{BaFe}_{2-x}\text{As}_2$, it is important to compare the calculation with neutron scattering experiments focusing on wave vector and energy dependence of the low-energy spin excitations. In this paper, we present a systematic inelastic neutron scattering and RPA/DFT study on $\text{BaFe}_{2-x}\text{Ni}_x\text{As}_2$ covering $x = 0.03, 0.065, 0.092, 0.1, 0.12, 0.15, 0.18$ shown as vertical arrows in the electronic phase diagram of Fig. 1(a).⁴¹ Consistent with earlier work,^{29–31,34} we find that low-energy spin excitations in $\text{BaFe}_{2-x}\text{Ni}_x\text{As}_2$ are anisotropic and form transversely elongated ellipses at the AF order wave vector. The peak widths in both the transverse and longitudinal directions increase linearly with x . For samples near optimal superconductivity, a neutron spin resonance appears below T_c . For samples at the overdoped side $x = 0.15$, the low-energy spin excitations form two transversely incommensurate peaks. Upon further increasing electron-doping x , the low-energy spin excitations vanish concurrently with the vanishing superconductivity. We compare these results with RPA/DFT calculations and find them to be qualitatively similar. These results indicate an intimate connection between spin excitations and superconductivity, thus suggesting spin excitations play an important role for superconductivity in iron pnictides.

II. EXPERIMENT

We carried out systematic neutron scattering experiments on $\text{BaFe}_{2-x}\text{Ni}_x\text{As}_2$ using the C5 thermal neutron triple-axis spectrometer at the Canadian Neutron Beam Center in Chalk River, Canada. The final neutron energy was set to $E_f = 14.56$ meV, with pyrolytic graphite (PG) as the monochromator, analyzer, and filters. The collimations were set to [none, 0.8° , 0.85° , 2.4°]. High quality single crystals up to centimeter sizes were grown by the FeAs self-flux method,⁴³ detailed procedure and sample characterization were published elsewhere.⁴⁴ We use the nominal composition to represent the Ni doping level x . We define the wave vector \mathbf{Q} at (q_x, q_y, q_z) as $(H, K, L) = (q_x a / 2\pi, q_y b / 2\pi, q_z c / 2\pi)$ reciprocal lattice units (r.l.u.) using the orthorhombic unit cell, where $a \approx b \approx 5.62$ Å, and $c = 12.77$ Å. In this reciprocal space notation, the colinear AF structure of the FeAs layer is shown in Fig. 1(b), and the in-plane AF Bragg peak position corresponding to the Fermi surface nesting occurs at $\mathbf{Q} = [1, 0]$ or $[0, 1]$ r.l.u. due to twinning. Based on previous work,⁴¹ we plot in Fig. 1(a) the schematic AF order and superconductivity schematic phase diagram.

For the experiment, we chose seven Ni-doping levels spanning from the non-SC to overdoped SC samples as marked by the vertical arrows in Fig. 1(a). These include $x = 0.03$ (lightly electron-doped non-SC sample with $T_N = 107$ K),⁴⁵ 0.065 (underdoped SC sample with $T_N = 72$ K and $T_c = 8$ K), 0.092 (nearly optimal doping SC sample with static incommensurate short-range order, $T_N = 45$ K and $T_c = 19$ K), 0.10 (optimal doping without AF order coexisting with superconductivity, $T_c = 20$ K), 0.12 (overdoped SC sample without AF order, $T_c = 19$ K), 0.15 (overdoped SC sample without AF order, $T_c = 14$ K), 0.18 (heavily overdoped SC sample without AF order, $T_c = 9$ K). In order to properly carry out inelastic neutron scattering experiments, we prepared 15 to 20 pieces of single crystals for each Ni-doping level and coaligned them using E3. The total sample mass of each Ni-doping level is

about 10–15 grams. Similar to previous work,³⁰ we aligned the samples in the $[H, 0, H]$ and $[0, -K, 0]$ scattering plane, where the c axis is about 23.5° from the scattering plane. In this geometry, we can probe the wave vector transfers both along the transverse and longitudinal directions near the in-plane AF positions $\mathbf{Q} = (1, 0, L)$ or $(0, 1, L)$ at $L = 0, 1$ as shown in Figs. 1(c) and 1(d). The coaligned samples are loaded inside a top loading close cycle refrigerator for easy exchange of samples.

In order to obtain a complete picture of the doping evolution of the low-energy spin excitations, we also include some results from our time-of-flight (TOF) inelastic neutron scattering experiments on the parent compound BaFe_2As_2 ,³⁶ optimally doped $x = 0.1$,³⁴ and overdoped compounds with $x = 0.15$. These TOF experiments were carried out on the MAPS and MERLIN TOF chopper spectrometers at the ISIS facility, Rutherford-Appleton Laboratory, UK.^{34,36} Part of the data in the $x = 0.10$ compound was collected on the TAIPAN thermal neutron triple-axis spectrometer at the Bragg Institute, Australian Nuclear Science and Technology Organization. Measurements were done with a fixed $E_f = 14.88$ meV by using a PG monochromator, filter, and analyzer.

To directly compare the neutron scattering results, we have also carried out RPA calculations based on a five-orbital tight-binding model.³⁵ The model is obtained by using a LDA calculation for $\text{BaFe}_{2-x}\text{Ni}_x\text{As}_2$, where the main effect of electron doping is to shift the chemical potential in a rigid band model.

III. RESULTS

We first describe the inelastic neutron scattering results on $\text{BaFe}_{2-x}\text{Ni}_x\text{As}_2$ for $x = 0.03$. In previous work on the $x = 0.04$ with $T_N = 91$ K and filamentary superconductivity, the effect of electron doping is found to reduce the c -axis exchange coupling in BaFe_2As_2 and induce quasi-two-dimensional spin excitations.⁴⁵ The anisotropy spin gaps at wave vectors

$\mathbf{Q} = (1, 0, 1)$ and $(1, 0, 0)$ were 2 and 4 meV, respectively.⁴⁵ For comparison, the AF Néel temperature of the system changes from $T_N = 138$ K for BaFe_2As_2 to $T_N = 107$ K for $\text{BaFe}_{1.97}\text{Ni}_{0.03}\text{As}_2$. In addition, there is no evidence for bulk superconductivity until $x = 0.05$. From recent inelastic neutron scattering work on BaFe_2As_2 , the spin-wave gaps at the Brillouin zone center and boundary are found to be near $\Delta(1, 0, 1) = 10$ and $\Delta(1, 0, 0) = 20$ meV, respectively.⁴⁶ Assuming that the nearest neighbors, next nearest neighbor, and c -axis magnetic exchange couplings are J_{1a} (J_{1b}), J_2 , and J_c , respectively,^{36,47} one can fit spin waves of BaFe_2As_2 using the Heisenberg Hamiltonian.³⁶ The anisotropic spin gaps are related to the exchange couplings via⁴⁵ $\Delta(1, 0, 1) = 2S[(J_{1a} + 2J_2 + J_c + J_s)^2 - (J_{1a} + 2J_2 + J_c)^2]^{1/2}$, $\Delta(1, 0, 0) = \Delta(0, -1, 0) = 2S[(2J_{1a} + 4J_2 + J_s)(2J_c + J_s)]^{1/2}$, where J_s is the magnetic single ion anisotropy and S is the magnetic spin ($S = 1$). For BaFe_2As_2 , the exchange couplings are estimated from global fitting of the in-plane high-energy spin waves using the Heisenberg Hamiltonian.³⁶ While the best fitting exchange energies are $SJ_{1a} = 59.2$ meV, $SJ_{1b} = -9.2$ meV, $SJ_2 = 13.6$ meV, $SJ_c = 1.8$ meV, and $SJ_s = 0.084$ meV, these results are obtained from high-energy in-plane spin wave dispersions and therefore cannot accurately determine the c -axis exchange energy. Recently, using the in-plane magnetic exchange couplings determined from the high-energy spin wave data³⁶ and more accurate measurements of $\Delta(1, 0, 1)$ and $\Delta(1, 0, 0)$, the effective c -axis exchange energy and the single ion anisotropy of BaFe_2As_2 are found to be $SJ_c = 0.22$ meV and $SJ_s = 0.14$ meV, respectively.⁴⁶ These results are consistent with our earlier estimations.⁴⁵

Figures 2(a) and 2(b) show the background subtracted energy scans $S(\mathbf{Q}, \omega)$ at the AF zone boundary $\mathbf{Q} = (0, -1, 0) \approx (1, 0, 0)$ and zone center $\mathbf{Q} = (1, 0, 1)$ for $\text{BaFe}_{1.97}\text{Ni}_{0.03}\text{As}_2$, where the background scattering was measured at $\mathbf{Q} = (0, -1.4, 0)$ and $\mathbf{Q} = (1.4, 0, 1.4)$, respectively. The low-temperature ($T = 3$ K) spin-wave gaps

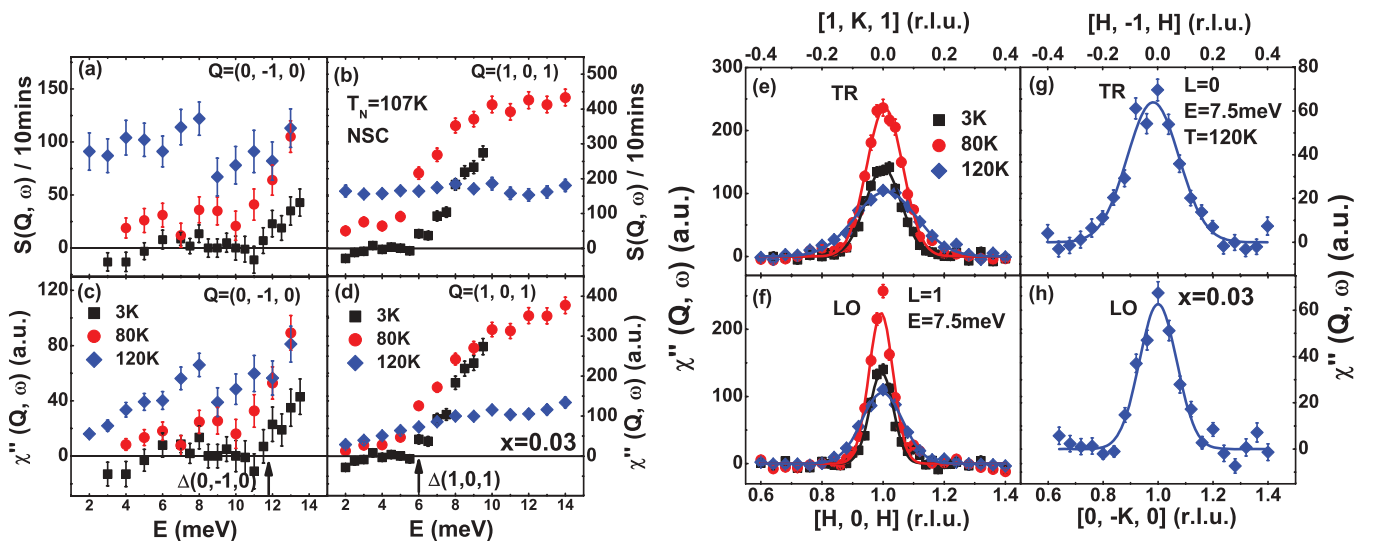


FIG. 2. (Color online) Low-energy spin excitations of the non-SC $\text{BaFe}_{2-x}\text{Ni}_x\text{As}_2$ ($x = 0.03$) with $T_N = 107$ K. (a) and (b) Energy dependence of $S(\mathbf{Q}, \omega)$ at $\mathbf{Q} = (0, -1, 0)$ and $\mathbf{Q} = (1, 0, 1)$ for $T = 3, 80, 120$ K, after subtracting the background at $\mathbf{Q} = (0, -1.4, 0)$ and $\mathbf{Q} = (1.4, 0, 1.4)$, respectively. (c) and (d) Dynamic spin susceptibility $\chi''(\mathbf{Q}, \omega)$ after considering the Bose factor for $L = 0$ and $L = 1$. (e)–(h) $\chi''(\mathbf{Q}, \omega)$ of constant energy scans at $T = 3, 80, 120$ K and $E = 7.5$ meV. The solid lines are gaussian fits to the data.

at the zone center and boundary decrease to $\Delta(1,0,1) = 5.5$ meV and $\Delta(0, -1,0) = 11$ meV, respectively [Figs. 2(a) and 2(b)]. Upon warming up to $T = 80$ K $\approx 0.75T_N$, the spin-gap values decrease rapidly for $\Delta(1,0,1)$ but remains large for $\Delta(0, -1,0)$. They completely vanish at $T = 120$ K $\approx 1.12T_N$ [Fig. 2(a)]. Figures 2(c) and 2(d) show the energy dependence of the imaginary part of the dynamic susceptibility, $\chi''(\mathbf{Q},\omega)$, estimated via $\chi''(\mathbf{Q},\omega) = [1 - \exp(-\hbar\omega/k_B T)]S(\mathbf{Q},\omega)$, where k_B is the Boltzmann constant. While the $\chi''(\mathbf{Q},\omega)$ shows clear spin-wave gaps at 3 K, it increases linearly with energy in the paramagnetic state at $T = 120$ K.

From the recent work on spin excitations of optimally electron-doped $\text{BaFe}_{1.9}\text{Ni}_{0.1}\text{As}_2$ superconductor,³⁴ we see that the high-energy spin excitations, and therefore the effective in-plane magnetic exchange energies, are not affected by electron-doping and superconductivity. Assuming that the in-plane magnetic exchange couplings in $\text{BaFe}_{1.97}\text{Ni}_{0.03}\text{As}_2$ are unchanged from those of the BaFe_2As_2 ,³⁶ we estimate $SJ_c = 0.066$ meV and $SJ_s \approx 0$ meV using the newly measured $\Delta(1,0,1)$ and $\Delta(1,0,0)$ values for $\text{BaFe}_{1.97}\text{Ni}_{0.03}\text{As}_2$ [Figs. 2(a) and 2(b)]. These results are consistent with the notion that electron-doping in $\text{BaFe}_{2-x}\text{Ni}_x\text{As}_2$ rapidly decreases the out-of-plane exchange couplings.⁴⁵

To explore the in-plane momentum distribution of the spin excitations in $\text{BaFe}_{1.97}\text{Ni}_{0.03}\text{As}_2$, we carried out constant-energy scans along the longitudinal $[H,0,H]$ and transverse $[0,-K,0]$ directions at $E = 7.5$ meV and various temperatures. Figures 2(e)–2(h) show $\chi''(\mathbf{Q},\omega)$ along different

directions at $T = 3, 80,$ and 120 K. Around the AF Bragg wave vector $\mathbf{Q} = (1,0,1)$, spin waves are weakly anisotropic, being broader along the transverse direction than that of the longitudinal direction [Figs. 2(e) and 2(f)]. The scattering intensity increases on warming to 80 K due to closing of the spin anisotropy gap. As expected, the spin excitations peak widths above T_N are broader than the widths of spin waves in the AF ordered state. For $L = 0$, we cannot find any magnetic scattering at $E = 7.5$ meV below T_N due to the presence of the spin gap. Transversely elongated paramagnetic scattering emerges at temperatures above T_N [Figs. 2(g) and 2(h)].

Figure 3 summarizes the constant-energy and constant- \mathbf{Q} scans for the electron underdoped $\text{BaFe}_{1.935}\text{Ni}_{0.065}\text{As}_2$ with $T_N = 72$ K and $T_c = 8$ K.^{41,44} Figures 3(a) and 3(b) show the background subtracted magnetic scattering in terms of energy scans at the AF wave vectors $\mathbf{Q} = (0, -1,0)$ and $\mathbf{Q} = (1,0,1)$ at various temperatures. Although resistivity and diamagnetic measurements show a SC phase transition below $T_c = 8$ K in this compound,⁴⁴ magnetic scattering $S(\mathbf{Q},\omega)$ at $\mathbf{Q} = (1,0,1)$ shows no temperature dependence across T_c (between 3 K and 12 K) in the energy range 2 meV $< E < 10$ meV, thus indicating no neutron spin resonance. Upon warming up to 80 K ($=T_N + 8$ K), the paramagnetic spin excitations at $\mathbf{Q} = (0, -1,0)$ and $\mathbf{Q} = (1,0,1)$ become L independent, in contrast to the larger magnetic scattering intensity at $\mathbf{Q} = (1,0,1)$ in the AF ordered state. Figures 3(c) and 3(d) show the corresponding $\chi''(\mathbf{Q},\omega)$ at $\mathbf{Q} = (0, -1,0)$ and $\mathbf{Q} = (1,0,1)$, respectively. In contrast to $\chi''(\mathbf{Q},\omega)$ for $\text{BaFe}_{1.97}\text{Ni}_{0.03}\text{As}_2$, the spin excitations

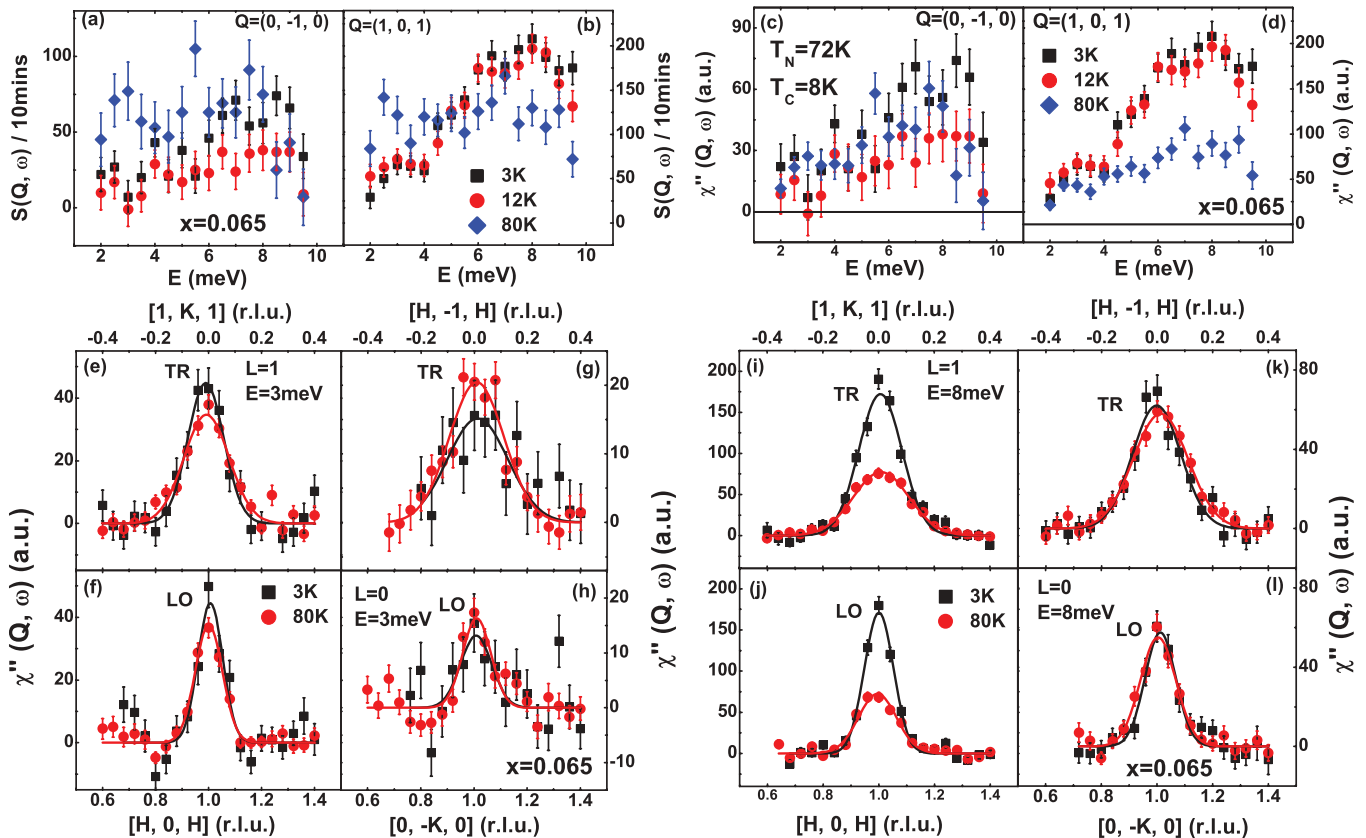


FIG. 3. (Color online) Low-energy spin excitations of the underdoped $\text{BaFe}_{2-x}\text{Ni}_x\text{As}_2$ ($x = 0.065$) with $T_N = 72$ K and $T_c = 8$ K. (a) Energy dependence of $S(\mathbf{Q},\omega)$ at $\mathbf{Q} = (0, -1,0)$ and (b) $\mathbf{Q} = (1,0,1)$ for $T = 3, 12, 80$ K. (c) and (d) Corresponding $\chi''(\mathbf{Q},\omega)$ for $L = 0$ and $L = 1$. (e)–(h) $\chi''(\mathbf{Q},\omega)$ of constant energy scans at $E = 3$ meV and (i)–(l) $E = 8$ meV for $T = 3$ K and 80 K.

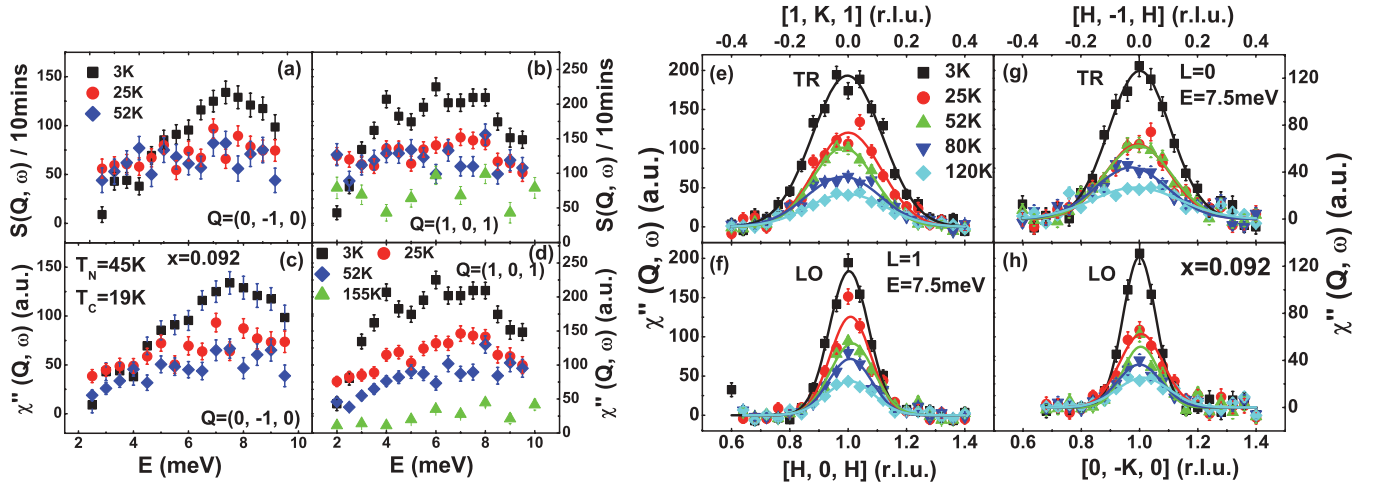


FIG. 4. (Color online) Low-energy spin excitations of the nearly optimal doped $\text{BaFe}_{2-x}\text{Ni}_x\text{As}_2$ ($x = 0.092$) with $T_N = 45$ K and $T_c = 19$ K. (a) Energy dependence of $S(\mathbf{Q}, \omega)$ at $\mathbf{Q} = (0, -1, 0)$ and (b) $\mathbf{Q} = (1, 0, 1)$ for $T = 3, 25, 52$ K and 155 K. (c) and (d) Corresponding $\chi''(\mathbf{Q}, \omega)$ for $L = 0$ and $L = 1$. (e) $\chi''(\mathbf{Q}, \omega)$ of constant energy scans at $T = 3, 25, 52, 80, 120$ K and $E = 7.5$ meV.

are gapless at all temperatures and increase approximately linearly with increasing energy.

Figures 3(e), 3(f), 3(g), and 3(h) show constant-energy scans below T_c (3 K) and above T_N (80 K) along the longitudinal and transverse directions at $E = 3$ meV and $L = 0, 1$. At $T = 3$ K, there is more magnetic scattering centered around $\mathbf{Q} = (1, 0, 1)$ than at $\mathbf{Q} = (0, -1, 0)$, suggesting the presence of intensity modulation along the c axis. On warming to 80 K above T_N , $\chi''(\mathbf{Q}, \omega)$ becomes similar at these two wave vectors. Figures 3(i), 3(j), 3(l), and 3(k) plot identical scans to those of Figs. 3(e)–3(h) at $E = 8$ meV. Similar to data at $E = 3$ meV, we see that the large differences in $\chi''(\mathbf{Q}, \omega)$ at $L = 1$ and 0 at 3 K essentially vanish on warming up to 80 K. These results suggest a weak L modulation of the paramagnetic scattering compared with spin waves below T_N . Comparing \mathbf{Q} -scan data at $E = 3$ and 8 meV, we see that the widths of transverse scans increase with increasing energy, consistent with earlier results on spin waves of BaFe_2As_2 .³⁶

We now examine spin excitations of $\text{BaFe}_{2-x}\text{Ni}_x\text{As}_2$ in a narrow regime where the transverse incommensurate AF order was found.⁴¹ For this purpose, we choose $\text{BaFe}_{1.908}\text{Ni}_{0.092}\text{As}_2$ which has $T_c = 19$ K and $T_N = 40$ K.⁴¹ Figures 4(a)–4(d) show energy dependence of the magnetic scattering $S(\mathbf{Q}, \omega)$ and $\chi''(\mathbf{Q}, \omega)$ at $\mathbf{Q} = (0, -1, 0)$ and $\mathbf{Q} = (1, 0, 1)$ below and above T_c . While $\chi''(\mathbf{Q}, \omega)$ at $\mathbf{Q} = (0, -1, 0)$ appears to increase approximately linearly with increasing energy at 25 and 52 K, the effect of superconductivity is to suppress low-energy spin excitations and induce a neutron spin resonance near $E = 7.5$ meV [Fig. 4(c)]. At $\mathbf{Q} = (1, 0, 1)$, $\chi''(\mathbf{Q}, \omega)$ behaves similarly except that the superconductivity induced resonance is rather broad in energy extending from 3 meV to 9 meV, giving a resonance energy of $E \approx 6$ meV [Fig. 4(d)]. These results are consistent with the earlier work.²⁸

Since elastic scattering in $\text{BaFe}_{1.908}\text{Ni}_{0.092}\text{As}_2$ forms static short-range transverse incommensurate AF order,⁴¹ it is interesting to see if one can also find incommensurate spin excitations. Figures 4(e)–4(h) summarize the transverse and longitudinal scans across the in-plane AF wave vector at $L = 1$ and 0 near the resonance energy of $E = 7.5$ meV. The intensity

gain of the neutron spin resonance below T_c is seen in both the transverse [Figs. 4(e) and 4(g)] and longitudinal scans [Figs. 4(f) and 4(h)]. Although the widths of transverse scans are much broader than that of the longitudinal scans, there is no evidence for incommensurate spin excitations at the resonance energy. On warming to higher temperatures, we see a gradual reduction of the magnetic scattering, and there is still no evidence for incommensurate spin excitations. In addition, the \mathbf{Q} widths of spin excitations are weakly temperature dependent below 120 K. Therefore, one can safely assume that the static short-range incommensurate AF order below $T_N = 40$ K has little impact on spin excitations of $\text{BaFe}_{1.908}\text{Ni}_{0.092}\text{As}_2$.

For optimally electron-doped $\text{BaFe}_{1.9}\text{Ni}_{0.1}\text{As}_2$ ($T_c = 20$ K),²³ since recent neutron TOF experiments³⁴ have already mapped out the wave vector and energy dependence of spin excitations throughout the Brillouin zone, we will not repeat them here but instead focus on temperature dependence of the energy scans at $\mathbf{Q} = (1, 0, 1)$. Figures 5(a) and 5(b) show the magnetic scattering $S(\mathbf{Q}, \omega)$ and $\chi''(\mathbf{Q}, \omega)$ at $T = 3, 25, 52$, and 159 K, respectively. While one can clearly see the presence of a spin gap and a resonance near $E \approx 7$ meV at 3 K, the normal state $\chi''(\mathbf{Q}, \omega)$ is gapless and increases linearly with increasing energy. The $\chi''(\mathbf{Q}, \omega)$ also decreases monotonically with increasing temperature.

Figure 6 summarizes the transverse and longitudinal scans around the resonance energy ($E = 7.5$ meV) for a slightly electron overdoped sample, $\text{BaFe}_{1.88}\text{Ni}_{0.12}\text{As}_2$ ($T_c = 19$ K). This sample has the same SC transition temperature as that of $\text{BaFe}_{1.908}\text{Ni}_{0.092}\text{As}_2$ but without static AF order. Similar to constant-energy scans in the underdoped samples, we again carried out transverse and longitudinal scans along the $[1, K, 1]$, $[H, -1, H]$ and $[H, 0, H]$, $[0, -K, 0]$ directions, respectively, below and above T_c . Inspection of Figure 6 immediately reveals the magnetic intensity gain at wave vectors $\mathbf{Q} = (1, 0, 1)$ and $\mathbf{Q} = (0, -1, 0)$ below T_c . We also note that the widths of transverse scans are considerably broader than that of the longitudinal scans. Again, there is no evidence for incommensurate spin excitations at the resonance energy to within our instrumental resolution.

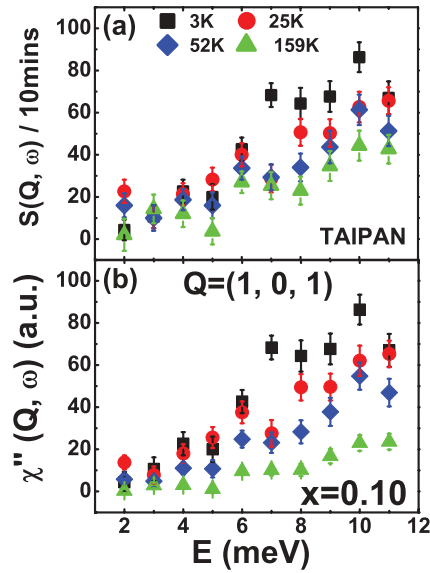


FIG. 5. (Color online) (a) and (b) Energy scans and corresponding $\chi''(\mathbf{Q}, \omega)$ at $\mathbf{Q} = (1, 0, 1)$ and $T = 3, 25, 52, 82, 159$ K for the optimally doped $\text{BaFe}_{2-x}\text{Ni}_x\text{As}_2$ ($x = 0.10$) with $T_c = 20$ K. These data are collected at TAIPAN triple-axis spectrometer in ANSTO.

Turning our attention to a more electron overdoped sample $\text{BaFe}_{1.85}\text{Ni}_{0.15}\text{As}_2$ with $T_c = 14$ K, we note that in previous polarized neutron scattering experiments on these samples,⁴⁸ spin excitations are found to be paramagnetic and isotropic in the space below and above T_c . In the normal state (20 K), the $\chi''(\mathbf{Q}, \omega)$ at $\mathbf{Q} = (1, 0, 1)$ is gapless and increases linearly with energy. Upon entering into the SC state (3 K), the $\chi''(\mathbf{Q}, \omega)$ has a small spin gap of ~ 2 meV and a neutron spin resonance at $E \approx 7$ meV.⁴⁸ Similarly, the $\chi''(\mathbf{Q}, \omega)$ at $\mathbf{Q} = (1, 0, 2)$ has a spin gap of ~ 2 meV and increases with increasing energy.⁴⁸ Since previous polarized neutron scattering experiments have already measured the energy dependence of the $\chi''(\mathbf{Q}, \omega)$ at AF wave vectors, we will not repeat them here but instead focus on the in-plane wave vector anisotropy of the resonance.

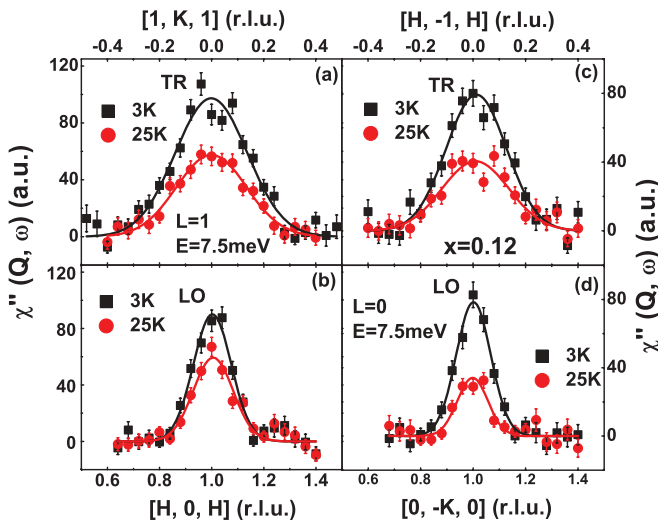


FIG. 6. (Color online) $\chi''(\mathbf{Q}, \omega)$ of constant energy scans at $T = 3, 25$ K and $E = 7.5$ meV for the slightly overdoped $\text{BaFe}_{2-x}\text{Ni}_x\text{As}_2$ ($x = 0.12$) with $T_c = 19$ K.

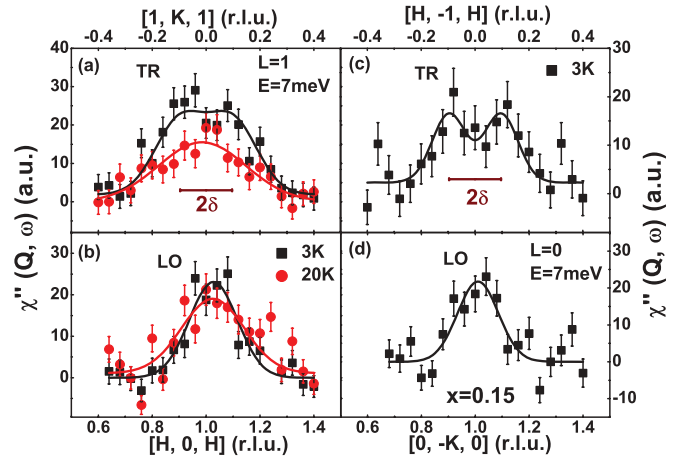


FIG. 7. (Color online) Low-energy spin excitations of the overdoped $\text{BaFe}_{2-x}\text{Ni}_x\text{As}_2$ ($x = 0.15$) with $T_c = 14$ K. (a)–(d) Constant energy scans at $T = 3, 20$ K and $E = 7$ meV, where the transverse scans at $T = 3$ K show a small incommensurability with $\delta = 0.098$.

Figures 7(a) and 7(b) show the transverse and longitudinal scans along the $[1, K, 1]$ and $[H, 0, H]$ directions below and above T_c at the resonance energy of $E = 7$ meV. While one can see an enhancement of magnetic scattering below T_c due to the resonance, the low-temperature (3 K) transverse scan also shows a flat top consistent with having two incommensurate peaks instead of one Gaussian. The transverse scan along the $[H, -1, H]$ direction confirms this conclusion and shows two clear incommensurate peaks at $(-\delta, -1, -\delta)$ and $(\delta, -1, \delta)$ with $\delta = 0.098$ [Fig. 7(c)]. On the other hand, longitudinal scans show commensurate peaks centered at the AF wave vector [Figs. 7(b) and 7(d)].

To further probe the possible incommensurate magnetic excitations, we carried out additional transverse scans at different energies and compare these results with cuts from the

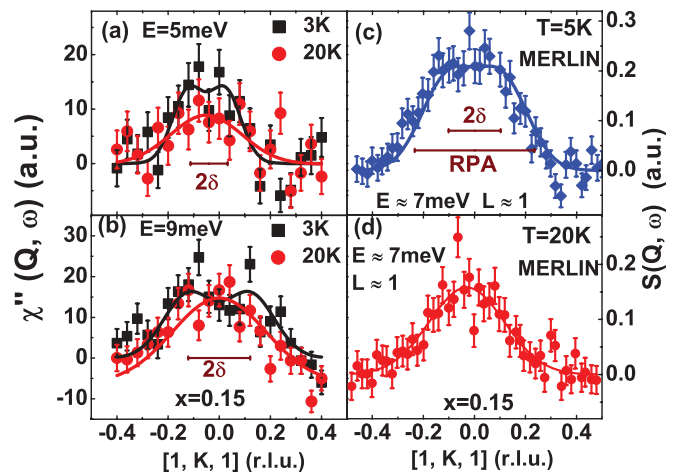


FIG. 8. (Color online) (a) and (b) Transverse \mathbf{Q} scans at $L = 1$, $E = 5$ and 9 meV below T_c and above T_c . (c) and (d) are constant energy cuts from the TOF data on MERLIN with an energy range of $6 \text{ meV} < E < 8 \text{ meV}$ and $0.7 < L < 1.3$ at $T = 5$ and 20 K. The center bar shows the incommensurability $\delta = 0.073, 0.121$ for $E = 5$ and 9 meV, $\delta = 0.102$ for the TOF cut around 7 meV, and $\delta = 0.235$ for RPA calculation, respectively.

neutron TOF measurements on the same sample. Figures 8(a) and 8(b) show transverse scans along the $[1, K, 1]$ direction at $E = 5$ and 9 meV, respectively. In the low-temperature SC state, there are two clear incommensurate peaks as shown by the solid line fits using two Gaussians. From these Gaussian fits to the data, we can obtain energy dependence of the incommensurability, giving $\delta = 0.073$ for $E = 5$ meV and $\delta = 0.121$ for $E = 9$ meV at 3 K. In addition, the incommensurate peaks appear to be more robust in the SC state. To confirm such a conclusion, we used a neutron TOF chopper spectrometer MERLIN at ISIS, Rutherford-Appleton Laboratory, to measure spin excitations in $\text{BaFe}_{1.85}\text{Ni}_{0.15}\text{As}_2$. The incident beam energy was set to $E_i = 25$ meV, and the sample was aligned such that the angles between \mathbf{k}_i and the c -axis were $\theta = 7^\circ, 11^\circ, 16^\circ$. The two-dimensional wave vector dependent profile of the spin excitations for $6 \text{ meV} < E < 8 \text{ meV}$ at $L = 1$ can be covered in this arrangement. The wave vector cuts at $E = 7$ meV obtained by Horace software using the combination of three sets of TOF data are shown in Figs. 8(c) and 8(d). In the SC state, the transverse scan has a flattish top consistent with the triple-axis data in Fig. 7(a). On warming to 20 K ($T = 6 + T_c$), the scattering shows a broad Gaussian centered around the AF ordering wave vector [Fig. 8(d)]. Although these results suggest that spin excitations of $\text{BaFe}_{1.85}\text{Ni}_{0.15}\text{As}_2$ change from the commensurate in the normal state to incommensurate in the SC state, it remains unclear if the commensurate-to-incommensurate transition occurs at T_c .

Finally, we have searched for spin excitations in heavily overdoped SC $\text{BaFe}_{1.82}\text{Ni}_{0.18}\text{As}_2$, which has no AF order and $T_c = 9$ K. For the experiment, we have coaligned about eight grams of single crystals. In spite of much efforts, we have been unable to find large enough magnetic scattering near the AF wave vector for energies around 8 meV. Although this does not mean that there is no magnetic scattering at this energy, it does suggest a dramatic reduction in magnetic scattering with increasing Ni doping in the overdoped regime.

Using a RPA for a three-dimensional 5-orbital tight-binding model for BaFe_2As_2 , we have carried out calculations of the RPA spin susceptibility $\chi''(\mathbf{Q}, \omega)$ for the normal state. This model was introduced by Graser *et al.*³⁵ and obtained from fits of the DFT band structure for BaFe_2As_2 . The RPA spin susceptibility $\chi''(\mathbf{Q}, \omega)$ is obtained from the RPA multiorbital susceptibility matrix $\chi_{l_1, l_2, l_3, l_4}^{\text{RPA}}$ for orbitals l_1, l_2, l_3 , and l_4 , which is related to the bare (Lindhard) susceptibility matrix $\chi_{l_1, l_2, l_3, l_4}^0$ and the Coulomb interaction matrix U through $\chi^{\text{RPA}}(\mathbf{Q}, \omega) = \chi^0(\mathbf{Q}, \omega)[1 - U\chi^0(\mathbf{Q}, \omega)]^{-1}$. The interaction matrix U in orbital space is defined in Graser *et al.*³⁵ and contains onsite matrix elements for the intra- and interorbital Coulomb repulsions U and U' , and for the Hund's-rule coupling and pair-hopping terms J and J' . For this calculation, we have used spin-rotationally invariant parameters $U' = U - 2J$ and $J' = J$ with $U = 0.8$ eV and $J = 0.2$ eV. The effect of Ni substitution in $\text{BaFe}_{2-x}\text{Ni}_x\text{As}_2$ is assumed to be electron doping via the rigid band shift.

The top row in Fig. 9 shows results of this calculation obtained for an energy $E = 8$ meV for different electron dopings. As the doping increases from (a) to (d), one clearly sees an enhancement of the anisotropy in spin excitations (transverse elongation), qualitatively similar to the experimental results. For a doping of $x = 0.15$, we find two transverse incommensurate peaks near the AF wave vector. The corresponding TOF and triple-axis inelastic neutron scattering measurements at $E = 8$ meV are shown in Figs. 9(e)–9(h).^{34,36} The data for $x = 0.065$ were mapped out on the C5 triple-axis spectrometer with $E = 8$ meV and $L = 1$ at $T = 3$ K [Fig. 9(f)]. Figure 9(e) is obtained by doing a \mathbf{Q} cut of energy range $7 \text{ meV} \leq E \leq 11 \text{ meV}$ from the $x = 0$ compound measured on MAPS at $T = 7$ K.³⁶ Figures 9(g) and 9(h) are \mathbf{Q} cuts of the energy range $6 \text{ meV} \leq E \leq 9 \text{ meV}$ for the optimal doped compound $x = 0.134$ and the overdoped compound $x = 0.15$ measured on MERLIN at $T = 5$ K, respectively. Spin excitations form transversely elongated ellipses that increase with increasing electron doping.

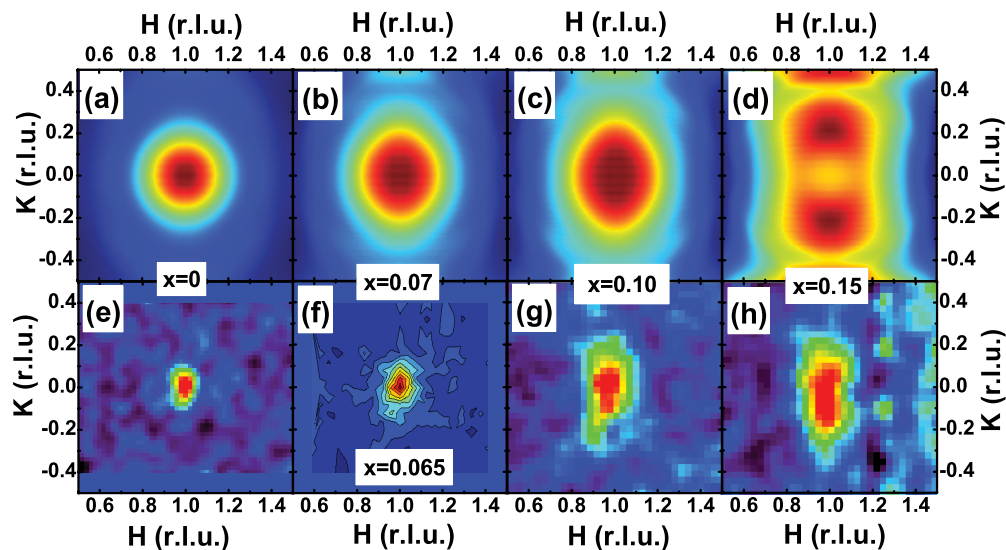


FIG. 9. (Color online) Comparison between the RPA calculation (a)–(d) and experimental results (e)–(h) of the in-plane anisotropic spin excitations in $\text{BaFe}_{2-x}\text{Ni}_x\text{As}_2$.

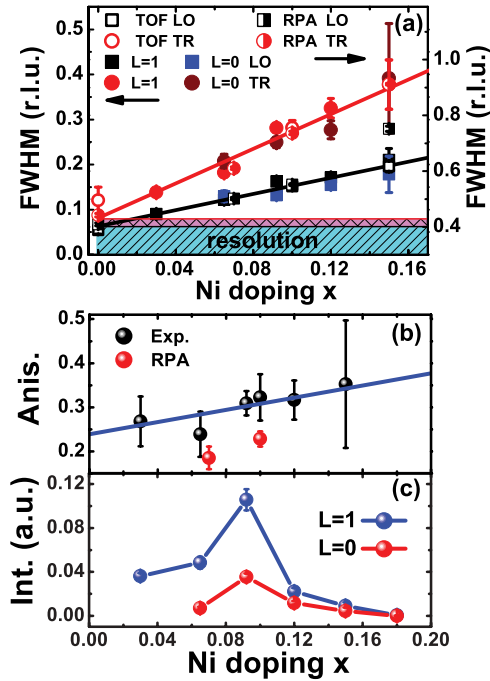


FIG. 10. (Color online) (a) Linear doping dependence of FWHM for the transverse and longitudinal wave vector scans. (b) Doping dependence of the in-plane anisotropy of spin excitations. (c) Doping dependence of peak intensity at $\mathbf{Q} = (0, -1, 0)$ and $(1, 0, 1)$ normalized by phonon intensity at $\mathbf{Q} = (2, 0.3, 2)$ and $T = 80$ K. The lines are guides to the eyes.

On initial inspection, it appears that the RPA calculated $\chi''(\mathbf{Q}, \omega)$ spectra in Figs. 9(a)–9(d) occupy a much larger portion of the Brillouin zone than that of the experimental results shown in Figs. 9(e)–9(h). In addition, the RPA calculated $\chi''(\mathbf{Q}, \omega)$ in full width half maximum (FWHM) and incommensurability δ are about a factor of two larger than that of the measurements. However, when the Ni-doping dependence of the FWHM from the fits to transverse and longitudinal scans was plotted in Fig. 10(a), we see a well-defined linear dependence of FWHM versus x for both directions at $L = 0$ and $L = 1$. These results are also consistent with the FWHM deduced from the TOF measurements discussed in Fig. 9. Although the RPA calculation gives the absolute values of FWHM that are about a factor of two larger than that of the experiments, the calculated spin excitation width also has a linear Ni-doping dependence consistent with the experiments. To estimate the electron-doping dependence of the intrinsic spin excitation \mathbf{Q} widths at $E = 8$ meV, we assume that spin waves in the parent compound BaFe_2As_2 are an instrumental resolution limited at $E = 8$ meV.³⁶ Gaussian fits to the scattering profiles along the longitudinal and transverse directions at $E = 8$ meV for BaFe_2As_2 give $R_{LO} = 0.0631 \pm 0.0037$ and $R_{TR} = 0.0811 \pm 0.0053$ r.l.u., respectively. These values are consistent with the calculated instrumental resolution and previous results on $\text{BaFe}_{2-x}\text{Co}_x\text{As}_2$.³⁰

Figure 10(a) shows the Ni-doping dependence of the longitudinal and transverse spin excitation widths at $E = 8$ meV. It is clear that the excitation widths increase linearly with increasing electron doping along both directions, but with a smaller slope along the longitudinal direction. This is con-

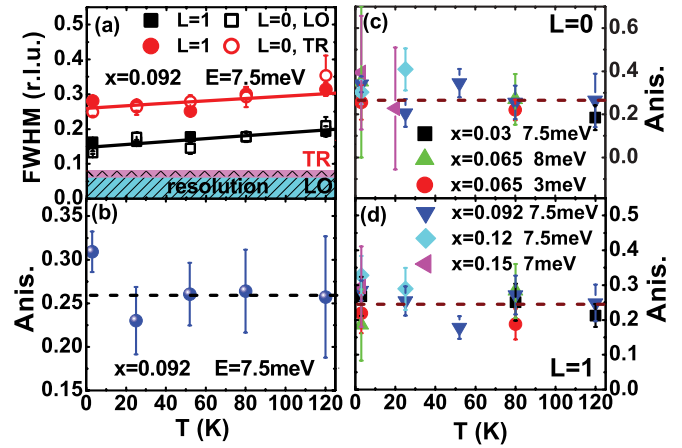


FIG. 11. (Color online) (a) and (b) Temperature dependence of FWHM for the transverse and longitudinal wave vector scans and the in-plane anisotropy for $\text{BaFe}_{2-x}\text{Ni}_x\text{As}_2$ ($x = 0.092$) at $E = 7.5$ meV. (c) and (d) Temperature dependence of in-plane anisotropy for all dopings at $L = 0$ and $L = 1$.

sistent with the electron-doping dependence of the $\chi''(\mathbf{Q}, \omega)$ from the RPA calculation (solid lines). Figure 10(b) plots the electron doping dependence of the spin excitation anisotropy ratio A , defined as $A = (W_{TR} - W_{LO}) / (W_{TR} + W_{LO})$ where W_{LO} and W_{TR} are intrinsic widths of spin excitations along the longitudinal and transverse directions, respectively. When the Ni-doping increases from $x = 0.03$ to 0.15, the measured spin excitation anisotropy increases slightly from 0.25 to 0.35. This is consistent with the RPA calculation, thus suggesting that the RPA calculation captures the essential physics in the doping dependence of the low-energy spin excitations. Figure 10(c) shows the Ni-doping dependence of the low-temperature integrated magnetic scattering near $E = 8$ meV, where we have normalized the scattering intensity for different doping levels via phonons at $\mathbf{Q} = (2, 0.3, 2)$ and 80 K, at $\mathbf{Q} = (1, 0, L)$ with $L = 0, 1$. We see that the magnetic scattering for over-doped samples decreases systematically with increasing doping, and appear to vanish around $x = 0.20$ near the overdoped border of the superconductivity dome [Fig. 1(a)]. This is consistent with previous nuclear magnetic resonance measurements on $\text{BaFe}_{2-x}\text{Co}_x\text{As}_2$, where the presence of the enhanced AF spin excitations appears to be intimately associated with the dome of superconductivity, and vanishes for overdoped sample without superconductivity.⁴⁹

To determine if the widths of spin excitations are affected by temperature, we show in Fig. 11(a) the temperature dependence of the FWHM of the longitudinal and transverse spin excitations for $\text{BaFe}_{1.908}\text{Ni}_{0.092}\text{As}_2$ at $E = 7.5$ meV. On warming from 3 K to 120 K, the spin excitation widths are essentially unchanged, and increase only slightly. Figures 11(b)–11(d) show that the spin excitation anisotropy ratio A is also temperature independent to within the errors of our measurements. This is consistent with earlier neutron scattering results on $\text{BaFe}_{1.85}\text{Co}_{0.15}\text{As}_2$.³⁰

IV. DISCUSSION AND CONCLUSIONS

Since the discovery of the static AF order in the parent compounds of iron-based superconductors,^{11–13} a central

question has been whether the static AF order and associated spin excitations can be entirely described by Fermi surface nesting between the hole pockets near Γ point and electron pockets M points of the Brillouin zone,^{50,51} or require local moments as in the case of copper oxide superconductors.^{52–55} From recent neutron scattering experiments on spin waves in BaFe_2As_2 ³⁶ and spin excitations in optimally electron doped $\text{BaFe}_{1.9}\text{Ni}_{0.1}\text{As}_2$,³⁴ we see that the effect of electron doping on BaFe_2As_2 modifies spin waves below 100 meV, and does not change high-energy spin excitations. These results suggest that spin excitations in $\text{BaFe}_{2-x}\text{Ni}_x\text{As}_2$ have both itinerant and localized components.³⁴ Given the general agreement on the evolution of the observed spin excitation anisotropy and the PRA calculations based on rigid band shift and itinerant electrons, one may assume that itinerant electrons and Fermi surface nesting only affect low-energy spin excitations, and high-energy spin waves and excitations arise mostly from local moments and electron correlations. These results are consistent with the idea that the transversely elongated spin excitations in $\text{BaFe}_{2-x}\text{Ni}_x\text{As}_2$ are mostly due to intraorbital, but interband, scattering processes in cases without perfect nesting.⁵⁶

The experimental observation of a rapid reduction in the spin wave anisotropy gap upon electron doping in $\text{BaFe}_{2-x}\text{Ni}_x\text{As}_2$ confirms the earlier results that the dominate effect of electron doping is to reduce c -axis spin exchange coupling and change three-dimensional spin waves into quasi-two-dimensional spin excitations.⁴⁵ Based on our systematic measurements of the transverse and longitudinal widths of spin excitations for different Ni-doping levels x , we find that the intrinsic excitation widths increase linearly with x . This is consistent with the RPA calculation assuming that the effect of Ni doping is to increase electron Fermi pocket size via rigid band shift. Although the RPA calculated spin susceptibility occupies a larger part of the Brillouin zone than that of the experiments, their electron-doping dependences are rather similar. These results suggest that itinerant electron picture and Fermi surface nesting can capture an important part of the

physics in these materials. Similar RPA calculations for much higher energy spin excitations ($E > 100$ meV) give results that disagree with our measurements, thus confirming the notion that the high-energy spin excitations in $\text{BaFe}_{2-x}\text{Ni}_x\text{As}_2$ may originate from the local moments instead of Fermi surface nesting and itinerant electrons.³⁴

In conclusion, we use inelastic neutron scattering to demonstrate the presence of anisotropic in-plane spin excitations at low energies in electron doped $\text{BaFe}_{2-x}\text{Ni}_x\text{As}_2$. The excitation widths in both the transverse and longitudinal directions increase linearly with doping level x , and having slightly larger slope in the transverse direction. In the overdoped side with $x = 0.15$, we find evidence for the low-energy transverse incommensurate spin excitations consistent with the RPA calculation. Therefore, the in-plane spin excitation anisotropy increases slightly with doping. For samples near optimal superconductivity, a neutron spin resonance appears below T_c . However, the intensity of spin excitations decreases with increasing doping for samples beyond optimal superconductivity, and vanishes near the overdoped border of the SC dome. Therefore, our data support the view that low-energy spin excitations are controlled by Fermi surface nesting and itinerant electrons, and are important for superconductivity of iron pnictides.

ACKNOWLEDGMENTS

We thank Jiangping Hu, Daoxing Yao, and Qimiao Si for helpful discussions. The work at the Institute of Physics, Chinese Academy of Sciences, is supported by the MOST (973 project: 2012CB821400, 2011CBA00110, and 2010CB833102) and NSFC (No. 11004233). The work at UTK is supported by the US National Science Foundation through Grant Nos. NSF-DMR-1063866 and NSF-OISE-0968226. T.A.M. acknowledges the Center for Nanophase Materials Sciences, which is sponsored at Oak Ridge National Laboratory by the Scientific User Facilities Division, Office of Basic Energy Sciences, US Department of Energy.

*pdai@utk.edu

¹D. J. Scalapino, *Phys. Rep.* **250**, 329 (1995).

²P. Monthoux, D. Pines, and G. G. Lonzarich, *Nature (London)* **450**, 1177 (2007).

³P. A. Lee, N. Nagaosa, and X.-G. Wen, *Rev. Mod. Phys.* **78**, 17 (2006).

⁴M. Fujita, H. Hiraka, M. Matsuda, M. Matsuura, J. M. Tranquada, S. Wakimoto, G. Y. Xu, and K. Yamada, *J. Phys. Soc. Jpn.* **81**, 011007 (2012).

⁵J. Zhao, F. C. Niestemski, S. Kunwar, S. L. Li, P. Steffens, A. Hiess, H. J. Kang, S. D. Wilson, Z. Wang, P. C. Dai, and V. Madhavan, *Nat. Phys.* **7**, 719 (2011).

⁶K. Jin, N. P. Butch, K. Kirshenbaum, J. Paglione, and R. L. Greene, *Nature (London)* **476**, 73 (2011).

⁷Y. Kamihara, T. Watanabe, M. Hirano, and H. Hosono, *J. Am. Chem. Soc.* **130**, 3296 (2008).

⁸M. Rotter, M. Tegel, and D. Johrendt, *Phys. Rev. Lett.* **101**, 107006 (2008).

⁹A. S. Sefat, R. Jin, M. A. McGuire, B. C. Sales, D. J. Singh, and D. Mandrus, *Phys. Rev. Lett.* **101**, 117004 (2008).

¹⁰L. J. Li, Y. K. Luo, Q. B. Wang, H. Chen, Z. Ren, Q. Tao, Y. K. Li, X. Lin, M. He, Z. W. Zhu, G. H. Cao, and Z. A. Xu, *New J. Phys.* **11**, 025008 (2009).

¹¹C. de la Cruz, Q. Huang, J. W. Lynn, J. Li, W. Ratcliff II, J. L. Zarestky, H. A. Mook, G. F. Chen, J. L. Luo, N. L. Wang, and P. Dai, *Nature (London)* **453**, 899 (2008).

¹²J. Zhao, Q. Huang, C. de la Cruz, S. Li, J. W. Lynn, Y. Chen, M. A. Green, G. F. Chen, G. Li, Z. Li, J. L. Luo, N. L. Wang, and P. Dai, *Nat. Mater.* **7**, 953 (2008).

¹³Q. Huang, Y. Qiu, W. Bao, M. A. Green, J. W. Lynn, Y. C. Gasparovic, T. Wu, G. Wu, and X. H. Chen, *Phys. Rev. Lett.* **101**, 257003 (2008).

¹⁴I. I. Mazin, *Nature (London)* **464**, 183 (2010).

¹⁵P. J. Hirschfeld, M. M. Korshunov, and I. I. Mazin, *Rep. Prog. Phys.* **74**, 124508 (2011).

¹⁶A. V. Chubukov, *Annu. Rev. Condens. Matter Phys.* **3**, 13 (2012).

- ¹⁷K. Kuroki, S. Onari, R. Arita, H. Usui, Y. Tanaka, H. Kontani, and H. Aoki, *Phys. Rev. Lett.* **101**, 087004 (2008).
- ¹⁸F. Wang and D. H. Lee, *Science* **332**, 200 (2011).
- ¹⁹T. A. Maier and D. J. Scalapino, *Phys. Rev. B* **78**, 020514(R) (2008).
- ²⁰T. A. Maier, S. Graser, D. J. Scalapino, and P. Hirschfeld, *Phys. Rev. B* **79**, 134520 (2009).
- ²¹M. M. Korshunov and I. Eremin, *Phys. Rev. B* **78**, 140509(R) (2008).
- ²²M. D. Lumsden, A. D. Christianson, D. Parshall, M. B. Stone, S. E. Nagler, G. J. MacDougall, H. A. Mook, K. Lokshin, T. Egami, D. L. Abernathy, E. A. Goremychkin, R. Osborn, M. A. McGuire, A. S. Sefat, R. Jin, B. C. Sales, and D. Mandrus, *Phys. Rev. Lett.* **102**, 107005 (2009).
- ²³S. Chi, A. Schneidewind, J. Zhao, L. W. Harriger, L. Li, Y. Luo, G. Cao, Zhuan Xu, M. Loewenhaupt, J. Hu, and P. Dai, *Phys. Rev. Lett.* **102**, 107006 (2009).
- ²⁴S. Li, Y. Chen, S. Chang, J. W. Lynn, L. Li, Y. Luo, G. Cao, Z. Xu, and P. Dai, *Phys. Rev. B* **79**, 174527 (2009).
- ²⁵D. K. Pratt, W. Tian, A. Kreyssig, J. L. Zarestky, S. Nandi, N. Ni, S. L. Bud'ko, P. C. Canfield, A. I. Goldman, and R. J. McQueeney, *Phys. Rev. Lett.* **103**, 087001 (2009).
- ²⁶A. D. Christianson, M. D. Lumsden, S. E. Nagler, G. J. MacDougall, M. A. McGuire, A. S. Sefat, R. Jin, B. C. Sales, and D. Mandrus, *Phys. Rev. Lett.* **103**, 087002 (2009).
- ²⁷D. S. Inosov, J. T. Park, P. Bourges, D. L. Sun, Y. Sidis, A. Schneidewind, K. Hradil, D. Haug, C. T. Lin, B. Keimer, and V. Hinkov, *Nat. Phys.* **6**, 178 (2010).
- ²⁸M. Y. Wang, H. Q. Luo, J. Zhao, C. L. Zhang, M. Wang, K. Marty, S. Chi, J. W. Lynn, A. Schneidewind, S. L. Li, and P. C. Dai, *Phys. Rev. B* **81**, 174524 (2010).
- ²⁹C. Lester, J.-H. Chu, J. G. Analytis, T. G. Perring, I. R. Fisher, and S. M. Hayden, *Phys. Rev. B* **81**, 064505 (2010).
- ³⁰J. T. Park, D. S. Inosov, A. Yaresko, S. Graser, D. L. Sun, Ph. Bourges, Y. Sidis, Yuan Li, J.-H. Kim, D. Haug, A. Ivanov, K. Hradil, A. Schneidewind, P. Link, E. Faulhaber, I. Glavatsky, C. T. Lin, B. Keimer, and V. Hinkov, *Phys. Rev. B* **82**, 134503 (2010).
- ³¹H.-F. Li, C. Broholm, D. Vaknin, R. M. Fernandes, D. L. Abernathy, M. B. Stone, D. K. Pratt, W. Tian, Y. Qiu, N. Ni, S. O. Diallo, J. L. Zarestky, S. L. Bud'ko, P. C. Canfield, and R. J. McQueeney, *Phys. Rev. B* **82**, 140503(R) (2010).
- ³²D. S. Inosov, J. T. Park, A. Charnukha, Yuan Li, A. V. Boris, B. Keimer, and V. Hinkov, *Phys. Rev. B* **83**, 214520 (2011).
- ³³M. Y. Wang, H. Q. Luo, M. Wang, S. Chi, J. A. Rodriguez-Rivera, D. Singh, S. Chang, J. W. Lynn, and P. Dai, *Phys. Rev. B* **83**, 094516 (2011).
- ³⁴M. S. Liu, L. W. Harriger, H. Q. Luo, M. Wang, R. A. Ewings, T. Guidi, H. Park, K. Haule, G. Kotliar, S. M. Hayden, and P. Dai, *Nat. Phys.* **8**, 376 (2012).
- ³⁵S. Graser, A. F. Kemper, T. A. Maier, H.-P. Cheng, P. J. Hirschfeld, and D. J. Scalapino, *Phys. Rev. B* **81**, 214503 (2010).
- ³⁶L. W. Harriger, H. Q. Luo, M. S. Liu, C. Frost, J. P. Hu, M. R. Norman, and P. Dai, *Phys. Rev. B* **84**, 054544 (2011).
- ³⁷J. H. Zhang, R. Sknepnek, and J. Schmalian, *Phys. Rev. B* **82**, 134527 (2010).
- ³⁸C. L. Zhang, M. Wang, H. Q. Luo, M. Y. Wang, M. S. Liu, J. Zhao, D. L. Abernathy, T. A. Maier, K. Marty, M. D. Lumsden, S. Chi, S. Chang, J. A. Rodriguez-Rivera, J. W. Lynn, T. Xiang, J. P. Hu, and Pengcheng Dai, *Scientific Reports* **1**, 115 (2011).
- ³⁹J.-P. Castellán, S. Rosenkranz, E. A. Goremychkin, D. Y. Chung, I. S. Todorov, M. G. Kanatzidis, I. Eremin, J. Knolle, A. V. Chubukov, S. Maiti, M. R. Norman, F. Weber, H. Claus, T. Guidi, R. I. Bewley, and R. Osborn, *Phys. Rev. Lett.* **107**, 177003 (2011).
- ⁴⁰D. K. Pratt, M. G. Kim, A. Kreyssig, Y. B. Lee, G. S. Tucker, A. Thaler, W. Tian, J. L. Zarestky, S. L. Bud'ko, P. C. Canfield, B. N. Harmon, A. I. Goldman, and R. J. McQueeney, *Phys. Rev. Lett.* **106**, 257001 (2011).
- ⁴¹H. Q. Luo, R. Zhang, M. Laver, Z. Yamani, M. Wang, X. Y. Lu, M. Y. Wang, Y. C. Chen, S. L. Li, S. Chang, J. W. Lynn, and P. C. Dai, *Phys. Rev. Lett.* **108**, 247002 (2012).
- ⁴²M. G. Kim, J. Lamsal, T. W. Heitmann, G. S. Tucker, D. K. Pratt, S. N. Khan, Y. B. Lee, A. Alam, A. Thaler, N. Ni, S. Ran, S. L. Bud'ko, K. J. Marty, M. D. Lumsden, P. C. Canfield, B. N. Harmon, D. D. Johnson, A. Kreyssig, R. J. McQueeney, and A. I. Goldman, [arXiv:1204.1538](https://arxiv.org/abs/1204.1538).
- ⁴³N. Ni, A. Thaler, J. Q. Yan, A. Kracher, E. Colombier, S. L. Bud'ko, P. C. Canfield, and S. T. Hannahs, *Phys. Rev. B* **82**, 024519 (2010).
- ⁴⁴Yanchao Chen, Xingye Lu, Meng Wang, Huiqian Luo, and Shiliang Li, *Supercond. Sci. Technol.* **24**, 065004 (2011).
- ⁴⁵L. W. Harriger, A. Schneidewind, S. L. Li, J. Zhao, Z. C. Li, W. Lu, X. L. Dong, F. Zhou, Z. X. Zhao, J. P. Hu, and P. C. Dai, *Phys. Rev. Lett.* **103**, 087005 (2009).
- ⁴⁶J. T. Park, G. Friemel, T. Loew, V. Hinkov, Y. Li, B. H. Min, D. L. Sun, A. Ivanov, A. Piovano, C. T. Lin, B. Keimer, Y. S. Kwon, and D. S. Inosov, [arXiv:1204.0875v1](https://arxiv.org/abs/1204.0875v1).
- ⁴⁷J. Zhao, D. T. Adroja, D.-X. Yao, R. Bewley, S. L. Li, X. F. Wang, G. Wu, X. H. Chen, J. P. Hu, and P. C. Dai, *Nat. Phys.* **5**, 555 (2009).
- ⁴⁸M. S. Liu, C. Lester, J. Kulda, X. Y. Lu, H. Q. Luo, M. Wang, S. M. Hayden, and P. C. Dai, *Phys. Rev. B* **85**, 214516 (2012).
- ⁴⁹F. L. Ning, K. Ahilan, T. Imai, A. S. Sefat, M. A. McGuire, B. C. Sales, D. Mandrus, P. Cheng, B. Shen, and H.-H. Wen, *Phys. Rev. Lett.* **104**, 037001 (2010).
- ⁵⁰I. I. Mazin, D. J. Singh, M. D. Johannes, and M. H. Du, *Phys. Rev. Lett.* **101**, 057003 (2008).
- ⁵¹J. Dong, H. J. Zhang, G. Xu, Z. Li, G. Li, W. Z. Hu, D. Wu, G. F. Chen, X. Dai, J. L. Luo, Z. Fang, and N. L. Wang, *Europhys. Lett.* **83**, 27006 (2008).
- ⁵²K. Haule, J. H. Shim, and G. Kotliar, *Phys. Rev. Lett.* **100**, 226402 (2008).
- ⁵³Q. Si and E. Abrahams, *Phys. Rev. Lett.* **101**, 076401 (2008).
- ⁵⁴C. Fang, H. Yao, W. F. Tsai, J. P. Hu, and S. A. Kivelson, *Phys. Rev. B* **77**, 224509 (2008).
- ⁵⁵C. Xu, M. Müller, and S. Sachdev, *Phys. Rev. B* **78**, 020501(R) (2008).
- ⁵⁶J. Zhang, R. Sknepnek, and J. Schmalian, *Phys. Rev. B* **82**, 134527 (2010).